

# TeraPool: A Physical Design Aware, 1024 RISC-V Cores Shared-L1-Memory Scaled-up Cluster Design with High Bandwidth Main Memory Link

Yichao Zhang, Marco Bertuletti, Chi Zhang, Samuel Riedel, Diyou Shen, Bowen Wang, Alessandro Vanelli-Coralli and Luca Benini

**Abstract**—Shared L1-memory clusters of streamlined instruction processors (processing elements - PEs) are commonly used as building blocks in modern, massively parallel computing architectures (e.g. GP-GPUs). *Scaling out* these architectures by increasing the number of clusters incurs computational and power overhead, caused by the requirement to split and merge large data structures in chunks and move chunks across memory hierarchies via the high-latency global interconnect. *Scaling up* the cluster reduces buffering, copy, and synchronization overheads. However, the complexity of a fully connected cores-to-L1-memory crossbar grows quadratically with PE-count, posing a major physical implementation challenge. We present TeraPool, a physically implementable, >1000 floating-point-capable RISC-V PEs scaled-up cluster design, sharing a Multi-MegaByte >4000-banked L1 memory via a low latency hierarchical interconnect (1-7/9/11 cycles, depending on target frequency). Implemented in 12 nm FinFET technology, TeraPool achieves near-gigahertz frequencies (910MHz) typical, 0.80 V/25 °C. The energy-efficient hierarchical PE-to-L1-memory interconnect consumes only 9-13.5 pJ for memory bank accesses, just 0.74-1.1 × the cost of a FP32 FMA. A high-bandwidth main memory link is designed to manage data transfers in/out of the shared L1, sustaining transfers at the full bandwidth of an HBM2E main memory. At 910 MHz, the cluster delivers up to 1.89 single precision TFLOP/s peak performance and up to 200 GFLOP/s/W energy efficiency (at a high IPC/PE of 0.8 on average) in benchmark kernels, demonstrating the feasibility of scaling a shared-L1 cluster to a thousand PEs, four times the PE count of the largest clusters reported in literature.

**Index Terms**—Manycore, RISC-V, Scalability, Physical Design Aware



## 1 INTRODUCTION

THE computing requirements of Generative Artificial Intelligence (AI), digital twins, 6G wireless networks, autonomous vehicles, and robots doubles every 6-9 months [1]. This exponential growth escalates to quadrillions of FLOPs and requires substantial memory capacity to manage massive high-speed data streams and Machine Learning (ML) models with trillions of parameters [2], [3]. The success in fast-paced adaptation, scale-up, and evolution of these AI-centric, data-intensive workloads relies on highly programmable high-performance hardware, with streamlined programming models and toolchains. Steadily increasing performance demands under tight power bounds, while maintaining a high degree of programming flexibility and ease-of-use, steers computing architectures toward flexible, but scalable and energy-efficient solutions [4], [5].

In this challenging context, many-core architectures with a large number of streamlined programmable Processing Elements (PEs) running at moderate (1-2 GHz) frequency, have achieved much higher efficiency than architectures based on a few large processors running at extremely high frequency (5+GHz) [6], [7]. The most common architectural building block in modern many-core designs is the cluster of PEs

tightly coupled with shared-L1 memory through a low-latency, high-bandwidth interconnect. However, the cluster is typically limited in scale to tens to low hundreds of PEs [8], [9], [10]. Beyond this number of PEs, performance is usually increased by scaling out (see Fig. 1b) to many loosely-coupled clusters, which access the main memory and other clusters' L1 memory through a high-latency global interconnect. However, loosely-coupled clusters imply hardware and software overheads, namely: synchronization, inter-cluster communication, data allocation-splitting, and workload distribution [11]. To contain these performance losses and enhance energy efficiency, directly scaling up (see Fig. 1a) the shared-L1 cluster is highly desirable [12]. For instance, NVIDIA's Graphics Processing Unit (GPU) architecture, which follows the shared-L1 architectural model, features clusters called Streaming Multiprocessors (SMs) with multi-threaded tensor cores sharing L1 data memories. From the A100 [13] to the H100 [14], the peak per-SM Floating Point (FP) computational power scaled up 4× by doubling the number of FP-PEs with increased processing rates. Additionally, the shared memory size expanded from 192 kB to 256 kB.

The PE to L1 memory interconnect design emerges as the main challenge to cluster scale-up from both the architectural and physical design viewpoints: (i.) The complexity of a baseline crossbar interconnect between PEs and memory banks would scale quadratically with the number of PEs and memory banks in the cluster [15], becoming a blocking factor in physical implementation. (ii.) Keeping low latency memory access in large-scale, unified-address, and physically

- Yichao Zhang, Marco Bertuletti, Chi Zhang, Samuel Riedel, Diyou Shen and Bowen Wang are with the Integrated Systems Laboratory (IIS), ETH Zurich, 8092 Zurich, Switzerland. E-mail: {yiczhang, mbertuletti, chizhang, sriedel, dishen, bowwang}@iis.ee.ethz.ch
- Luca Benini and Alessandro Vanelli-Coralli are with the IIS, ETH Zurich, and also with the Department of Electrical, Electronic and Information Engineering (DEI), University of Bologna, 40126 Bologna, Italy. E-mail: {lbenini, avanelli}@iis.ee.ethz.ch.

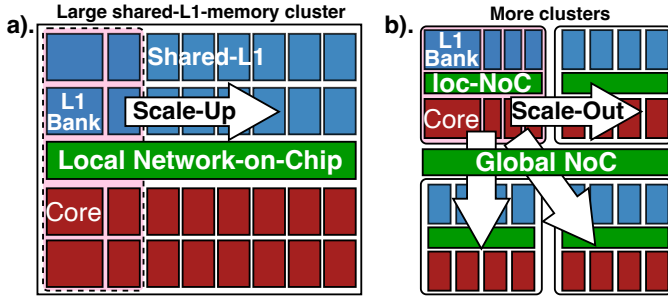


Figure 1. Illustration of scaling-up and scaling-out in cluster(s) design.

distributed banks is essential for minimizing PE stalls and ensuring high computing utilization. (iii.) In addition, the requirement also provides a link between the L1 memory within a cluster and the rest of the memory hierarchy further straining the physical routing resource budget. Therefore, preserving the cluster’s Power, Performance and Area (PPA) while scaling up requires carefully balancing the physical feasibility and interconnect performance. These interconnect design challenges have so far limited cluster scale-up to tens or, at most, hundreds of PEs [16].

We present TeraPool, a physically feasible, energy-efficient, general-purpose, and programming-friendly many-core cluster design. We break the current scale-up barrier, achieving 1000-PEs shared-L1 cluster, while maintaining near-GHz frequencies and delivering TFLOP/s performance. Extending our earlier work [17], we presents the following contributions:

- A large scale shared-L1 cluster design, based on a hierarchical crossbar interconnect, 4 times larger than the largest reported in the literature [16], featuring 1024 PEs (RV32IMAF cores) sharing 4 MiB (4096 banks) of L1 Scratchpad Memory (SPM);
- An Average Memory Access Time (AMAT) model of the hierarchical crossbar interconnect between PEs and memory banks. The model’s insight drives the design and optimization of a three-level hierarchical PE-L1 interconnect (*Tile*, *SubGroup*, and *Group*), achieving Non-Uniform Memory Access (NUMA) latencies of 1-5 cycles within a Group and up to 7-11 cycles for remote Group access, depending on the target operating frequency;
- A High Bandwidth Memory Link (HBML) supporting data movement in and out of the cluster’s L1 banks with negligible overhead. Co-simulated with an open-source, cycle-accurate *DRAMsys5.0* memory model [18] with hybrid address mapping scheme, our HBML achieves upto 97% bandwidth utilization of an industry-standard High Bandwidth Memory (HBM2E);
- The performance evaluation across key data-parallel kernels, demonstrates TeraPool’s capability on large data chunks with minimal data-transfer overhead.
- A detailed physical design methodology, floorplan and PPA analysis in GlobalFoundries’ 12 nm FinFET technology.

The remainder of this paper is structured as follows: Section 2 details the motivation for scaling up shared-L1 cluster. Section 3 introduces the AMAT modeling for hierarchical PE-to-L1 interconnect, evaluating the design choices through latency, throughput, and physical routing complexity. Section 4 describes the core-complex design and hierarchical cluster architecture. Next, Section 5 discusses HBML design, the

*DRAMsys5.0* co-simulation, and the hybrid memory address mapping scheme. The physical implementation and PPA analysis is detailed in Section 6. In Section 7, we present the TeraPool’s streamlined programming model and software performance. Finally, Section 8 and Section 10 discuss related work and conclusions, respectively. Our design, including open *DRAMsys5.0* model support and the full software infrastructure, is open-sourced under a liberal license <sup>1</sup>.

## 2 SHARED-MEMORY CLUSTER SCALE-UP VS. SCALE-OUT

In this work, *Cluster* refers to a computing block where PEs share L1-memory through a low-latency interconnect. Its main design parameters are summarized in Table 1. This section discusses the scaling strategies, highlighting the benefits and trade-offs from: (i.) scaling up in a single cluster, and (ii.) scaling out to multiple clusters.

Table 1  
Cluster Design Parameters Description

Symbol	Description
$L$	Main memory latency (cycle)
$W$	Problem-tiling size in L1 memory (word)
$BW$	Bandwidth between cluster&main memory (words/cycle)
$AI$	Arithmetic intensity (operations/word)
$N_{PEs}$	Number of processing elements in a cluster
$U$	Computing utilization of a processing element
$S$	Scaling factor for PEs and memory banks in the cluster

### 2.1 Single Cluster Scale-up

Since the problem size typically exceeds the cluster’s L1 memory capacity, tiling is commonly adopted: large data structures are split into chunks and moved in L1. Scaling up the cluster increases the number of processing elements and the total shared-L1 capacity for larger problem tiling, while the larger die area accommodates more I/Os, enabling higher  $BW$  between L1 and main memory. We analyze two workload cases to show the scale-up benefits:

- ① For workloads **without** data reuse, the  $AI \leq 1$  typically leads to performance being main-memory bound. Small clusters may need extra inter-cluster data transfers. Additionally, larger data chunks improve workload balance across PEs, reduce synchronization overhead, and increase resilience to main memory latency and bandwidth jitter.
- ② For workloads **with** data reuse, a larger L1 capacity reduces cluster to main-memory  $BW$  demands. Consider an example Matrix Multiplication (MatMul), where each matrix chunk has dimension  $m$ ,  $W = 3m^2$  and  $AI = m^3/3m^2 = \sqrt{W}/3\sqrt{3}$ . During cluster scaling by a factor of  $S$ ,  $W$  scales linearly, leading to an increase in  $AI$  that reflects greater data reuse, given by:

$$W' = S \times W, AI' = \frac{\sqrt{SW}}{3\sqrt{3}} = \sqrt{S} \times AI \quad (1)$$

Following the *Kung’s Principle* [19], the cluster is not bottlenecked by main memory bandwidth and latency when Equation (2) holds: considering cluster scaling by

1. <https://github.com/pulp-platform/mempool>

a factor  $S$ , we assume  $L$  and  $U$  remain constant due to identical design elements. The left-hand side represents the data transfer costs, where both  $W$  and  $BW$  scale with  $S$  and their ratio remains unchanged. The right-hand side reflects computational demand; the ratio of  $N_{PEs}$  to  $W$  remains unchanged as both scale with  $S$ , while  $AI$  increases with  $\sqrt{S}$ , improving the compute-to-memory balance.

$$L + \frac{W}{BW} < \frac{\sqrt{S}AI \times W}{N_{PEs} \times U} \quad (2)$$

This reveals that as the scaling factor  $S$  increases, the inequation holds for larger  $L$  and smaller  $BW$ , demonstrating that large-scale shared-L1-memory clusters are better equipped to maintain high computational utilization while tolerating main memory large transfer latency and limited bandwidth.

## 2.2 Scale-out to Multiple Clusters

As an alternative to the scale-up strategy, several smaller clusters can be instantiated, each accessing main memory and other clusters through global interconnects, representing a loosely coupled scale-out architecture (Fig. 1b). Compared with equivalent computing and memory resources in cluster scaling up, scaling out to a multi/many-cluster system costs computational and power overheads, leading to underutilized hardware components and reduced energy efficiency [20]. We identify three common overheads that increase with the scaling factor:

- **Synchronization Overhead:** The processing times across clusters are hard to perfectly balance due to independent instruction flows, L1-memory refill ordering, and main memory access conflicts. This uneven utilization between clusters leads to synchronization overhead that increases with the number of clusters due to long tail effects [21].
- **Tiling Overhead:** Problem-tiling across loosely coupled clusters introduces additional computational overhead during data structure splitting and partial results merging across memory hierarchies. For instance, the *Model Parallel* [22] adopted in Deep Neural Networks (DNNs) parallelization requires partial result reduction sums, where the execution time increases with the cluster counts.
- **Data Transfer Overhead:** Problem-tiling often leads to data duplication, as shared data must be copied to each cluster. Additionally, partial results from each cluster must be merged by transferring back to the main memory and then redistributed for subsequent processing through a high-latency global interconnect. These factors reduce the clusters' memory utilization and introduce data transfer overheads that grow with the number of clusters [17].

Additionally, connecting multiple clusters to main memory requires a high-latency global Network on Chip (NoC), incurring additional hardware overhead. A substantial die area is devoted to inter-cluster NoC routing, which consequently reduces area utilization and power efficiency [23].

These considerations motivate our exploration of efficient cluster scale-up, aiming to achieve high compute utilization with physically feasible interconnects.

## 3 INTERCONNECT DESIGN

Bandwidth and latency are the key performance metrics in the design of the PEs-to-L1 interconnect. Maintaining low latency

ensures that PE can hide it by issuing a low number of non-blocking L1 memory accesses, thereby preventing Load Store Unit (LSU) stalls and maintaining high utilization. Although high diameter NoC topologies with low-cardinality switches can achieve high clock speed, they are not optimal for the PEs to L1-memory interconnect, because latency increases by a few cycles per hop. This leads to PE throughput degradation, because too many outstanding memory transactions need to be supported to hide the NoC latency [24]. Ideally, the shortest latency is achieved by a fully-combinational and Fully-Connected (FC) logarithmic-staged crossbar<sup>2</sup> [15], providing single-cycle data transfer between the PEs and SPM banks. The handshaking protocol has forward requests including the address, data write, and control signals, and backward responses containing the request ID, read data, and acknowledgment signals. Simultaneous requests on the same arbitration switch are handled by a round-robin strategy.

Unfortunately, it has been shown [25] that while the crossbar is latency-optimal, its quadratic wire routing complexity poses insurmountable obstacles to achieving high frequencies. Ultimately, excessively large crossbars become non-routable during physical design. Hence, we need to find a compromise between latency, operating frequency, and physical routability. We resort to a hierarchical design. The hierarchical pattern builds upon basic building blocks, called *Tiles* (in Fig. 2), where a FC crossbar links a physically neighboring group of PEs to L1 SPM banks. In higher hierarchy levels *Tiles* are grouped, and PEs access the L1 banks of other *Tiles* via remote access ports. These ports connect to Tile-Tile crossbar(s) in the next hierarchy level, forming a fully shared-memory cluster. Pipeline registers are introduced at hierarchy boundaries to mitigate long physical paths and improve operating frequency at the price of increased latency. This pattern leads to a NUMA architecture in which both the request and response paths feature complete arbitration.

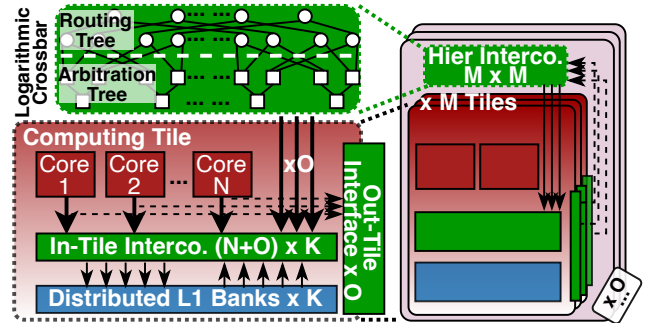


Figure 2. The hierarchical *Tile* (building block) design with logarithmic-staged crossbar interconnect.

In this section, we present the AMAT model of the hierarchical PE-to-L1 interconnect. Furthermore, we leverage the model's insights and explore the physical design feasibility of various hierarchical design choices, demonstrating the optimal configuration for building an extremely scaled-up cluster with 1024 cores shared 4096 L1-SPM banks.

<sup>2</sup> A logarithmic-staged tree topology; routing/arbitration implemented by demultiplexers/multiplexers with combinational logic control provides fine-grained address interleaving and single-cycle latency.

### 3.1 Hierarchical Interconnect AMAT Model

The AMAT modeling analysis is conducted from the *Tile* perspective where the memory requests are received, with the relevant parameters summarized in Table 2. Memory requests originate from either *local-Tile* (requests sent from PEs within the same Tile) or *remote-Tile* (requests sent from PEs in other Tiles). Considering uniformly distributed random address requests, the probability that a request is sent from the PEs within its local-Tile, denoted as  $P_{Ltile}$ , is given by  $1/N_{Tiles}$ . The cluster's AMAT, which contributes from both crossbar contention and pipeline registers, is computed as a probability-weighted sum of the latencies from each source, as shown in the equation below:

$$\begin{aligned} T_{cluster} &= P_{Ltile} \cdot L_{Ltile} + P_{Rtile} \cdot L_{Rtile} \\ P_{Rtile} &= 1 - P_{Ltile} = 1 - \frac{1}{N_{Tiles}} \\ L_{L/Rtile} &= E_{L: n \times k} + L_{pipeline} \end{aligned} \quad (3)$$

Contention in the logarithmic-staged crossbar arises when multiple requests traverse the same arbitration tree node, targeting the same hierarchical port, thereby introducing an additional cycle of latency for each request due to arbitration. This contention latency  $E_{L: n \times k}$  can be modeled based on the probability of multiple requests passing through the same arbitrator node within a single cycle.

Table 2  
interconnect Modeling Parameter Descriptions

Symbol	Description
$N_{Tiles}$	Number of building blocks ( <i>Tiles</i> ) in a cluster
$T_{cluster}$	Cluster's AMAT when all PEs perform random address access
$P_{Ltile/Rtile}$	Probability that a memory request originates from the local/remote Tile
$L_{Ltile/Rtile}$	Memory access latency for requests sending from the local/remote Tile
$L_{pipeline}$	Latency introduced by pipeline registers
$n, k$	Number of crossbar inputs, outputs
$p$	Request injection rate at crossbar input
$P_{req}(x)$	Probability that $x$ requests are sent to an arbitrator in a single cycle
$E_{L: n \times k}$	Expected latency for random target access through an $n \times k$ crossbar

Our analysis begins with a simple arbitrator and extends to a multi-stage hierarchical crossbar design. First, a basic  $N$ -to-1 arbitrator model forms the foundation of the contention analysis. The arbitrator model is based on a Binomial( $n, p$ ) distribution, where each input is considered an independent random trial, with  $n$  representing the number of inputs and  $p$  the probability of a request. The Probability Mass Function (PMF)  $P_{req}(x)$  of binomial distribution represents the probability that  $x$  requests are sent to the arbitrator within a cycle. With  $x$  initiators sending a request, the latency is  $x - 1$ . The latency for no requests ( $x = 0$ ) is zero, as no access is present in the arbitrator. To compute the expected latency, we sum the probabilities of having  $x = 1 \rightarrow n$  requests per cycle:

$$E_{L: n \times 1} = \sum_{x=1}^n L(x)P_{req}(x) = \sum_{x=1}^n (x-1)P_{req}(x) \quad (4)$$

Second, we expand this analysis to an  $n$ -to- $k$  arbitrator model. When a fully random address request is received, the

probability of it being forwarded to watch-point output where directed to the observed Tile is  $\frac{1}{k}$ . The number of requests arriving at the same output still follows a Binomial( $n, p/k$ ) distribution with an injection rate of  $p$ , while the remaining output ports form an  $n$ -to- $(k-1)$  arbitrator. Consequently, the expected latency must be calculated using a recursive method. If no request arrives at the watch-point output ( $x = 0$ ), it is redirected to other outputs, contributing to an increase in the average latency, with a latency of  $E_{L: n \times (k-1)}$ . The PMF for the average contention-cost latency can be expressed as:

$$E_{L: n \times k} = \begin{cases} E_{L: n \times 1} + P_{req}(0)E_{L: n \times (k-1)}, & k > 1 \\ \sum_{x=1}^n (x-1)P_{req}(x), & k = 1 \end{cases} \quad (5)$$

Finally, to analyze the multi-stage hierarchical interconnect crossbars, the probability of a request arriving at the input of each stage is determined by the probability that the request was forwarded from the output of the previous stage:

$$p^{stage(N)} = P_{req}^{stage(N-1)} = 1 - P_{req}^{stage(N-1)}(0) \quad (6)$$

To enhance the accuracy of the AMAT calculation under conditions where multiple contentions remain unresolved within a single cycle, pending requests dynamically adjust the crossbar's injection rate. We introduce input queues at each hierarchical crossbar stage<sup>3</sup> to simulate request queuing for dynamic injection rate adjustments.

### 3.2 TeraPool Interconnect Analysis

In this subsection, we analyze various hierarchical multi-stage crossbar interconnect designs to determine the optimal TeraPool architecture, extremely scaled-up to 1024 PEs with 4096 shared-L1 banks. We evaluate the interconnect performance based on the following metrics:

- **Zero-load latency:** The average latency cycles for a single random-address memory request without arbitration contention or input queuing. It is computed as the sum of each hierarchical access latency weighted by its access probability, reflecting the ideal latency of the interconnect.
- **AMAT:** The average latency cycles taken for all PEs to send random-address memory requests in the same cycle, factoring in arbitration contention and pipelining cycles, which are discussed in the previous subsection.
- **Throughput:** The maximum requests injection rate through interconnect, expressed as req/pe/cycle. During continuous request injection,  $L_{pipeline}$  can be hidden but throughput decreases caused by arbitration contention, as  $1/E_{L: n \times k}$ .
- **Interconnect complexity:** The number of crossbar leaf nodes across internal routing and arbitration stages reflects routing complexity, and is approximated as  $n \times k$ .
- **Combinational delay:** The number of routing levels. Requests traverse  $\log_2 n$  stages of the routing tree to reach one of the  $n \times k$  leaf nodes, followed by  $\log_2 k$  levels of arbitration switches to the target memory bank. This delay is approximated as  $\log_2 n + \log_2 k$ .

Moreover, to assess the physical feasibility of the most complex stage in the hierarchical crossbar (referred to as *Critical Complex*. in Table 4), we evaluate routing congestion for interconnect complexity ( $n \times k$ ) ranging from 256 to 4096,

3. Our modeling with input queues is performed using Python 3.7 scripts.

Table 3  
Routing Quality of Logarithmic-Staged Crossbar Interconnect at Different Complexities (GF12nm, 13M)

Interco. Complexity	Congestion*			Area (kGE)	Critical Path (ns)
	H	V	Overall		
256	0.13%	0.07%	0.10%	109	0.59
512	0.26%	0.11%	0.19%	196	0.73
1024	0.56%	0.12%	0.34%	361	0.91
1280	1.72%	0.47%	1.09%	503	1.06
1536	3.25%	0.82%	2.04%	669	1.08
2048	34.46%	15.09%	24.77%	923	1.13
3072	172.30%	294.31%	233.31%	1274	1.27
4096	247.10%	368.90%	308.00%	1485	1.47

\*The average routing track overflow rate for horizontal, vertical layers, and overall design.

using GlobalFoundries' 12 nm FinFET technology with 13 metal stacks. As shown in Fig. 3 and Table 3, when complexity <2048, the interconnect remains routable. Each doubling in complexity increases the area and the wires by  $1.8\times$ , and the critical path delay by  $<1.3\times$ . Beyond 2048, routing becomes infeasible, resulting in 25-308% ( $12.4\times$ ) Back-End-of-Line (BEOL) resource overflow, coupled with increased critical path delays that constrain cluster performance.

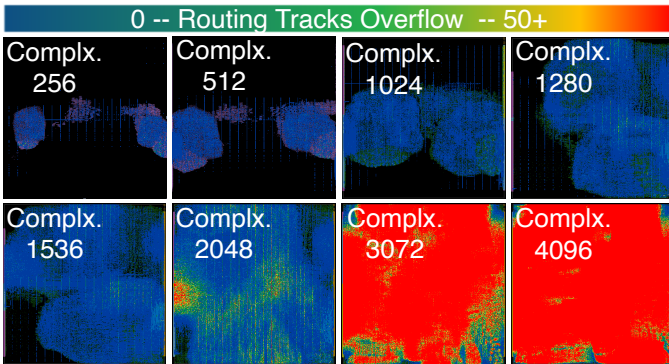


Figure 3. Routing Congestion of Logarithmic-Crossbar-Based Interconnect at Different Complexities (GF12nm, 13M).

Table 4 presents the comparisons of different hierarchical choices to connect 1024 PEs to 4096 L1 memory banks through multi-stage FC crossbar, ranging from a flat (non-hierarchical) to a three-level hierarchy implementation, highlighting the trade-offs between physical feasibility and interconnect performance.

First, the flat design ( $1024C$ ) results in an extremely large Place and Route (PnR) implementation block, where 1024 PEs are FC to 4096 banks through only single crossbar. Although it offers high throughput and 1-cycle (the lowest) memory access latency, it is physically infeasible due to the unrealistic interconnect complexity. Introducing the *Tile* hierarchy ( $\alpha C-\beta T$ ) helps mitigate complexity, but the high routing complexity of inter-*Tiles* crossbar still makes the physical routing infeasible. The AMAT increases because the majority of memory requests are directed to remote *Tiles* and require arbitration at the *Tile* boundaries. The arbitration rate increases with the number of PEs per *Tile*, further reducing interconnect throughput.

Second, by introducing the *Group* level of the hierarchy, we have a two-stage crossbar interconnect ( $\alpha C-\beta T-\delta G$ ), reducing the complexity of critical interconnect nodes by further splitting, and improving physical routing feasibility. This

choice is a trade-off: it reduces throughput and increases in both AMAT and zero-load latency. In physical implementation, flattening the *Tiles* into *Group* helps fully leverage the available BEOL resources and simplify interconnect routing across over the *Tiles* without requiring manual port placement. However, implementing 4 large-scale *Groups*, each comprising 256 PEs and 1024 banks, still remains unfeasible due to the significant design effort required for timing and routing optimization, will be described in detail in Section 6.1. Additionally, the physically-extended path length limits the achievable design frequency. Designing a cluster with more than 4 *Groups* introduces significant floorplan challenges, making it unachievable to arrange the placement of *Groups* to ensure short diagonal access paths while balancing inter-*Group* connections across varying physical distances with same number of pipeline cycles.

Last, we adopt a three-level hierarchical design by dividing each *Group* into *SubGroups* ( $\alpha C-\beta T-\gamma SG-\delta G$ ), while maintaining 4 hierarchical blocks ( $\gamma = \delta = 4$ ) at each implementation level to ensure balanced diagonal access paths. To achieve a physically feasible design while maintaining low latency and high throughput, the optimal configuration for the TeraPool cluster consists of 4 *Groups*, each containing 4 *SubGroups* of 8 *Tiles*, with 8 PEs per *Tile*, as shown in Fig. 6.

## 4 TERAPOOL CLUSTER ARCHITECTURE

This section details architecture design elements of TeraPool, emphasizing the physical design awareness for building the hierarchical implementation from the bottom up.

### 4.1 Processing Elements

TeraPool's PEs are single-issue, single-stage RISC-V *Snitch* cores based on the *RV32IMA* Instruction Set Architecture (ISA) [17], where instructions are decoded and executed within the core in a single cycle. *Snitch* has a private, fully associative, Standard Cell Memory (SCM)-based 32-instruction L0-Instruction Cache (I\$), designed for fast repetition of the computation hot loops. We build the *Snitch* Core-Complex (CC) with ISA extensions, including the *Xpulpimg*<sup>4</sup> implemented in the Integer Processing Unit (IPU), and the *zfinx*, *zhinx*, and *smallfloat* [26] implemented in the Floating Point Sub-System (FP-SS). To address the stringent area constraints typical of many-core compute clusters, we eliminate the need for a costly dedicated FP register file and LSU by executing FP and half-precision operands directly from the integer register file, while supporting parallel operations on two half-types using a Single Instruction Multiple Data (SIMD) approach.

On the memory access side, *Snitch* supports non-blocking instruction execution to tolerate multi-cycle L1-memory access latency. The load and store instructions have their dependencies recorded by the scoreboard, with a transaction table to track their retirement, shown in Fig. 4. The outstanding memory requests are tracked in a transaction table, enabling the core to issue a series of loads and stores without blocking while waiting for responses, and eventually proceed to other instructions with no data dependencies. Given TeraPool's NUMA interconnect design, the transaction table retires loads

4. The *Xpulpimg* extension includes domain-specific instructions [16], e.g., Multiply Accumulate (MAC) and load-post-increment.

Table 4  
Hierarchical Interconnect Design Analysis for 1024 PEs Fully Connect 4096 L1-Memory Banks

Hierarchy Interco.	Interconnect Quality						Design Challenge			
	ZeroLd (cyc)	AMAT (cyc)	Throughput (req/pe/cyc)	Total Complex.	Critical Complex.	Critical Comb. Delay	Physical Routing	Path Balance	Base Block Scale	Interco. Perform.
1024C	1.000	1.130	0.885	4194304	4194304	22				
4C-256T	2.992	6.081	0.245	87040	65536	16				
8C-128T	2.984	10.075	0.124	54272	16384	14				
16C-64T	2.969	18.077	0.062	74752	4096	12				
4C-16T-16G	4.867	5.318	0.431	163840	320	8.3				
4C-32T-8G	4.742	5.443	0.409	122880	1024	10				
8C-16T-8G	4.734	5.794	0.358	90112	512	9				
8C-32T-4G	4.484	6.676	0.272	69632	1024	10				
16C-8T-8G	4.719	6.669	0.273	110592	1536	10.6				
16C-16T-4G	4.469	8.612	0.178	90112	1280	10.3				
4C-16T-4SG-4G	6.367	8.457	0.270	121856	4096	12				
8C-8T-4SG-4G	6.359	9.198	0.230	89088	1024	10				
16C-4T-4SG-4G	6.344	11.049	0.159	109568	1536	10.6				

\*4096 1 KiB SPM banks are split across each hierarchy with PEs, using a banking factor of 4.

\*The hierarchy is denoted as  $\alpha C-\beta T-\gamma SG-\delta G$ , where  $\delta$  is the number of Groups, each with  $\gamma$  SubGroups,  $\beta$  Tiles per SubGroup, and  $\alpha$  PEs per Tile.

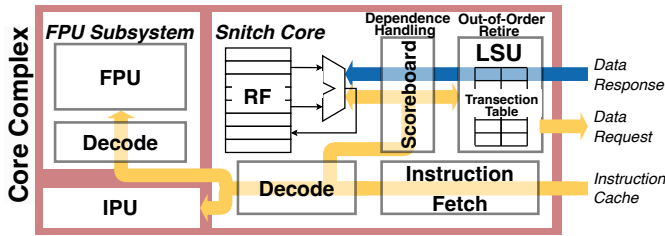


Figure 4. Block diagram of the Snitch highlighting the LSU, and the LSU's transaction table marking outstanding load and stores.

out-of-order, while the scoreboard ensures in-order delivery to the execution units. By scheduling multiple loads with loop unrolling, we can thus hide the memory access latency within the Cluster's L1 SPM. The number of supported outstanding transactions is hardware configurable, and it is chosen at the break-even point where the number of entries avoids excessive area overhead and further performance gains are limited by the number of ISA registers available. We found that 8 is an adequate number of outstanding transactions for most kernels, for instance, in a blocked MatMul algorithm [27], a  $4 \times 4$  output matrix block—the maximum supported by 32 ISA registers—requires at most 8 input transactions.

Snitch's small hardware footprint, latency tolerance, and extensibility make it an ideal candidate for implementing a tunable large-scale shared L1-memory many-core design.

## 4.2 Cluster Design

The *Tile* in Fig. 5 is the base hierarchical level, connecting 8 CCs to 32 banks of the shared SPM via a FC crossbar, providing single-cycle, zero-load access latency. The shared 4 KiB two-way set-associative L1-I\$ is shared by all *Snitch* cores within a *Tile* and feeds the L0-I\$. To support FP division and square root instructions (essential for operations like matrix inversion but less frequently used than basic FP operators), we share a single FP Division and Square Root (DIVSQRT) unit among four CCs, according to a round-robin policy. Each *Tile* has 7 ports to the L1-interconnect: one connects to other *Tiles* within the same *SubGroup* via an  $8 \times 8$  FC crossbar; three connect to *Tiles* in the other 3 *SubGroups* within the same *Group* via three  $8 \times 8$  FC crossbars; and the remaining 3 connect to *Tiles* in the 3

remote *Groups* via three  $32 \times 32$  FC crossbars. Our interconnect delivers a peak bandwidth of 4 KiB/cycle and a bisection bandwidth of 1.875 KiB/cycle across hierarchical levels.

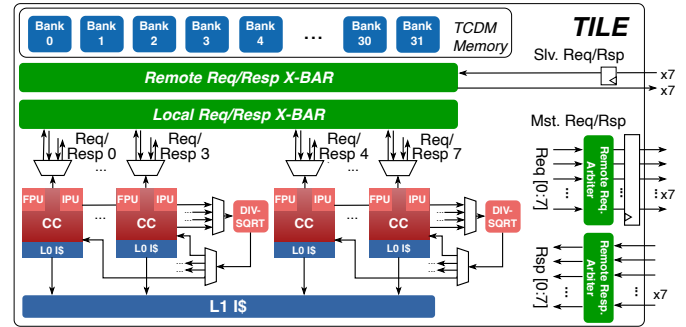


Figure 5. Block diagram of Tile: 8 core-complexes, 2 shared FP-DIVSQRT units; a local crossbar for 1-cycle access to tightly coupled data memory (TCDM), and 7 Remote Req/Resp ports connect to higher-level hierarchies.

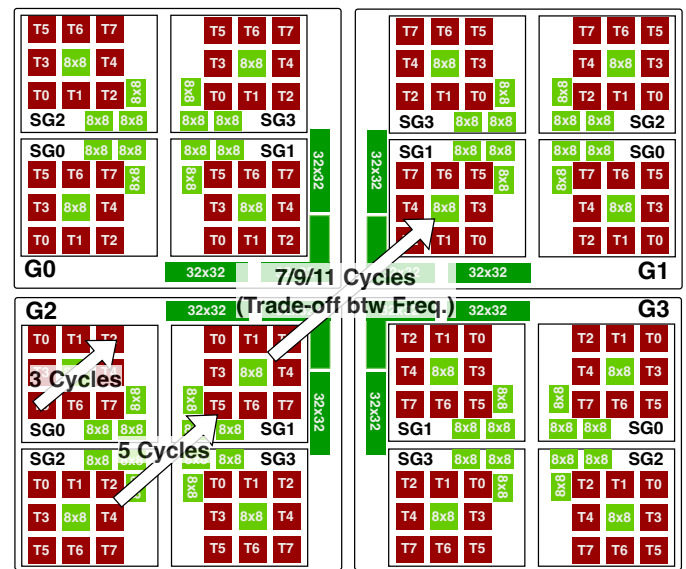


Figure 6. Cluster-level block diagram with layout view of Tiles and interconnect crossbars, highlighting the complexity of each hierarchical crossbar and L1 memory access latency.

The hierarchical interconnect design provides flexibility in

adding spill registers to break long remote access paths. Spill registers are placed on the *master request* and *response* ports at the issuing and target *Tile* boundaries, as well as after the crossbar on outgoing master ports. This results in a round-trip access latency of 3 cycles within a *SubGroup* and 5 cycles for access to other *SubGroups* within the same *Group*. The latency for remote-*Group* access is hardware-parameterizable and depends on the target operating frequency. We identify the configurations by subscripts, which indicate the latency of a core access to each hierarchy level. In TeraPool<sub>1-3-5-7</sub>, a register is added on both the request and response paths for each slave port at the *Cluster* level, increasing remote-*Group* access round-trip latency by 2 cycles. The TeraPool<sub>1-3-5-9</sub> configuration adds spill registers on the slave ports at the *Group* hierarchy level and the TeraPool<sub>1-3-5-11</sub> configuration adds a register also on the master paths. The full *Cluster*-level overview with *Tiles* layout is shown in Fig. 6. These configurations represent a trade-off between achievable frequency and L1 worst-case latency, which will be analyzed in Section 6.

## 5 HIGH BANDWIDTH MEMORY LINK

We introduce HBML, the main memory access interface, which comprises the Direct Memory Access (DMA) engine and system-level global interconnect. To evaluate TeraPool's HBML capability, we utilize the open-source, cycle-accurate *DRAMsys5.0* simulator [18] for main memory co-simulation.

### 5.1 Hierarchical AXI Interconnect

The HBML interconnect uses the open and standard Advanced eXtensible Interface (AXI4) protocol, connecting the TeraPool cluster to main memory and serving as the system-level interface for peripherals, host control, and Control and Status Registers (CSRs). However, providing high-bandwidth connections for each software-managed, physically-addressed L1 SPM bank poses a significant challenge due to limited physical routing resources, particularly in designs already constrained by PE-to-L1 routing complexity.

To minimize area and routing overhead, we use the tree-like AXI4 HBML interconnect in Fig. 7. Each *Tile* shares a single 512 bit AXI4 master port among its *Snitch* cores. Core requests are routed through a demultiplexer controlled by the target address, directing them either to the L1 SPM interconnect or to system-level components. The AXI4 interconnect is also used for L0 I\$ refills. Within each *SubGroup*, the AXI4 ports from 8 *Tiles* are arbitrated in a tree-like structure, connecting to a single 512 bit AXI4 master port. Finally, the 16 AXI4 masters from each *SubGroup* pass through address-based system demultiplexers, directing them to the DMA frontend (discussed in Section 5.2), L2 main memory or memory controller, and CSRs/peripheral interfaces.

### 5.2 Modular DMA engine

Although the TeraPool cluster distributes its L1 SPM banks across a large-scale hierarchical design, it maintains a unified physical address space. As a result, only one DMA engine is required to manage software-controlled data transfers between L1 and L2 main memory. However, utilizing a single traditional DMA engine presents challenges related to module placement and the need to establish connections to all 4096

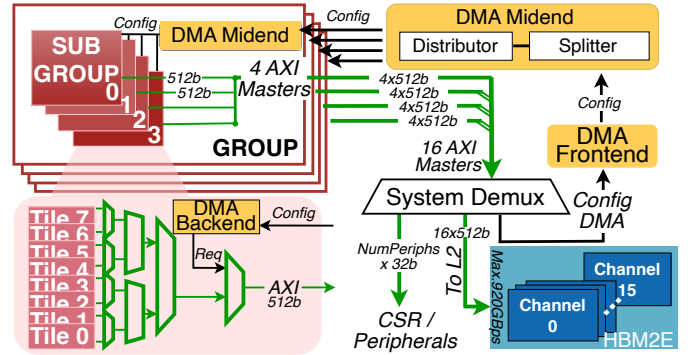


Figure 7. System-level high-bandwidth memory link design, featuring the hierarchical AXI4 interconnect and modular DMA engine.

SPM banks, resulting in significant routing complexity. On the other hand, implementing multiple DMA engines would complicate programming, requiring developers to manage transfer address ranges across different DMA units.

To simplify the programming interface and reduce routing complexity, we employ a modular iDMA [28] divided into three components: *frontend*, *midend*, and *backend*. The *frontend* initiates data transfers by specifying the source and destination address, and transfer size. Transfer requests are then forwarded to the *midend*, where they are divided into sub-tasks based on the L1 address boundaries of the *SubGroups*. These sub-tasks are allocated to DMA *backends*, which manage data transfers between the L2 main memory and the system AXI4 interconnect. Additionally, the *backends* bridge the system-level interconnect and the L1 SPM crossbar, enabling efficient data delivery to individual banks.

### 5.3 Main Memory

To demonstrate the capability of managing high bandwidth data flows by TeraPool's HBML, we utilize the open-source *DRAMsys5.0* simulator [18], a cycle-accurate framework based on *SystemC TLM-2.0* for Dynamic Random-Access Memory (DRAM) subsystems. We configure main memory with two DRAM stacks, each with 8 Micron MT54A16G808A00AC-36 HBM2E channels, which support 2.8/3.2/3.6 Gbit/s/pin Double Data Rate (DDR) transmission.

Co-simulation with the *DRAMsys5.0* HBM2E subsystem requires compiling a C++/*SystemC*-based Register-Transfer Level (RTL) cluster model. The compilation process for a large-scale cluster is extremely time-consuming, particularly during hardware development iterations, where every architectural tuning necessitates recompiling the entire model. To address this inefficiency, we compile the configured *DRAMsys5.0* model into a *Dynamic Link Library*, compatible with RTL simulators such as *QuestaSim* and *VCS*. This approach significantly accelerates design development, enabling rapid architectural tuning. We open-source our *DRAMsys5.0* dynamic linkable library simulation environment<sup>5</sup>.

### 5.4 Memory Mapping Scheme

The TeraPool employs a hybrid addressing scheme, as shown in Fig. 8 left. The 4 MiB L1 SPM is divided in a *sequential region*

5. [https://github.com/pulp-platform/dram\\_rtl\\_sim](https://github.com/pulp-platform/dram_rtl_sim)

and an *interleaved region* (respectively 512 KiB and 3.5 MiB by default, but configurable at design time). In the *sequential region*, memory requests are kept within a *Tile* to minimize latency and power consumption, allowing programmers to store private data, such as the stack, locally in the PE's *Tile*. In the *interleaved region*, a word-level interleaved memory mapping is applied across all memory banks. Data is evenly distributed among all PEs, minimizing average access latency and reducing bank conflicts. The zero-load latency for a core accessing the interleaved address space and the average latency assuming a random access pattern are on the right of Fig. 8. This approach mitigates the performance and power overheads of remote accesses with minimal hardware cost: wire crossings and a multiplexer to scramble the corresponding portion of the request address bits. Furthermore, interleaving makes access patterns independent of SPM bank size, which can be flexibly configured at design time.

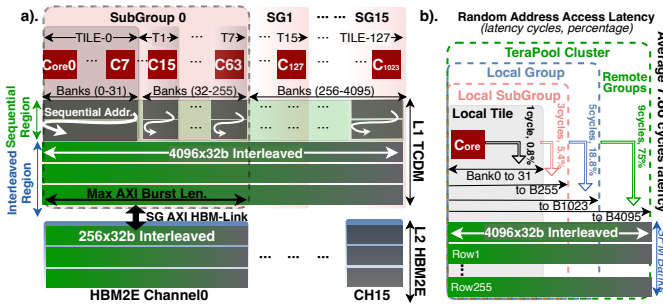


Figure 8. a). Hybrid memory address mapping scheme. b). Access latency when a core randomly accesses L1 memory banks across hierarchy levels.

In each *SubGroup*, the data in the *interleaved region* is distributed across 256 banks, with each bank-row storing a 32 bit word. Thus, when transferring data to or from L2 main memory via the HBML, the maximum size of a contiguous address data transfer through a single AXI4 burst is 256 32 bit words, handled by the *SubGroup*'s AXI4 master. To maintain this maximum burst request length and improve transferring efficiency, we configure 1 DMA *backend* per *SubGroup* to avoid further request splitting. We align the L2 main memory data interleaving granularity with the AXI4 burst length, configuring 256 32 bit words interleaved per HBM2E channel. This alignment mitigates burst splitting when requested data from a single burst spans multiple HBM2E channels and reduces system interconnect conflicts caused by different AXI4 master requests crossing into separate HBM2E channels.

To fully utilize the main memory bandwidth (described in Section 5.3), which supports configurable DDR rates of 716.8-921.6 GB/s, the target implementation frequency of TeraPool is set to 700-900 MHz to align with the HBM2E peak bandwidth, leveraging HBML's  $16 \times 512$  bit AXI4 interfaces. To validate this analysis, we explore TeraPool at both 500 MHz and 900 MHz, performing intensive data transfers (input&output) across the full 4 MiB cluster memory under various HBM2E DDR rate configurations. The results are shown in Fig. 9. At the lower frequency target (500 MHz), bandwidth is constrained by TeraPool's operating frequency, utilizing 61.8%-49.4% of peak HBM2E bandwidth. In contrast, at 700-900 MHz, all three corresponding HBM2E DDR configurations achieve near-peak utilization (97%), reaching up to 896 GB/s at 900 MHz. The slight bandwidth loss

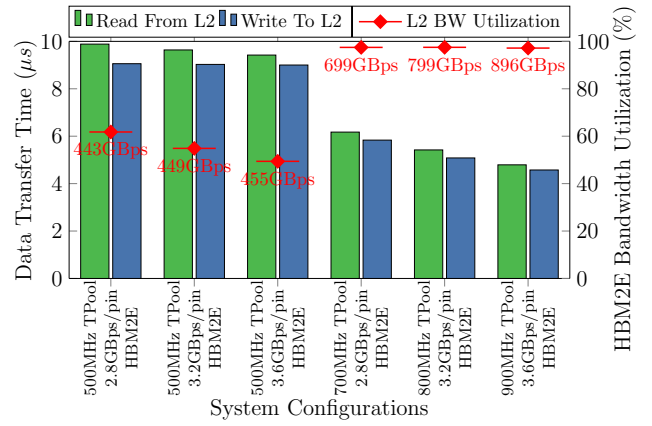


Figure 9. Data transfer performance for TeraPool's L1 read/write of 4 MiB of data, managed by HBML, from/to 16 HBM2E channels serving as L2 main memory.

is attributed to DMA *frontend* configuration cycles and unavoidable DRAM refresh periods. This analysis further motivates TeraPool design target to near-GHz frequency, and demonstrates TeraPool's HBML capability to efficiently manage high-bandwidth, long-latency data transfers, even with industry-standard HBM2E exhibiting hundred-cycle latencies as main memory.

## 6 PHYSICAL IMPLEMENTATION

In this section, we present the details of TeraPool's physical design. The TeraPool cluster is implemented within a die area of 81.8 mm<sup>2</sup> using *GlobalFoundries*' 12 nm LP+ FinFET process with a 13-metal layer stack. We use *Synopsys*' *Fusion Compiler 2022.03* to synthesize, place, and route. Our multi-level FC interconnect design is well-suited to the bottom-up implementation flow: it defines clear boundaries for each hierarchical block and allows the addition of spill registers for timing control. We determine the power consumption under typical operating conditions (TT/0.80 V/25 °C) using *Synopsys*' *PrimeTime 2022.03* and referring to switching activities obtained from a post-layout gate-level simulation.

### 6.1 Design Feasibility and Floorplan

To validate our analysis in Section 3.2 of the substantial Electronic Design Automation (EDA) efforts required for large-scale base-block implementation, which result in unmanageable runtimes and degraded optimization performance, we implement the 16C-8T-8G hierarchical configuration (refer to Table 4). Fig. 11 presents the relative EDA tools' runtime breakdown for the implementation of a TeraPool Group. For the non-implementable 16C-8T-8G hierarchical configuration, the total relative EDA tools' runtime is nearly 3.5× that of TeraPool<sub>1-3.5-9</sub>, with timing optimization accounting for more than 80% of the effort. Specifically, the routing stage is 5.5× slower than the other configurations. Despite these high design optimization efforts, the eight 16 × 16 interconnects in the Group design introduce significant routing congestion, leading to numerous metal shorts. Furthermore, routing detours considerably increase the length of timing paths, making it impossible to close the design with a 500 MHz

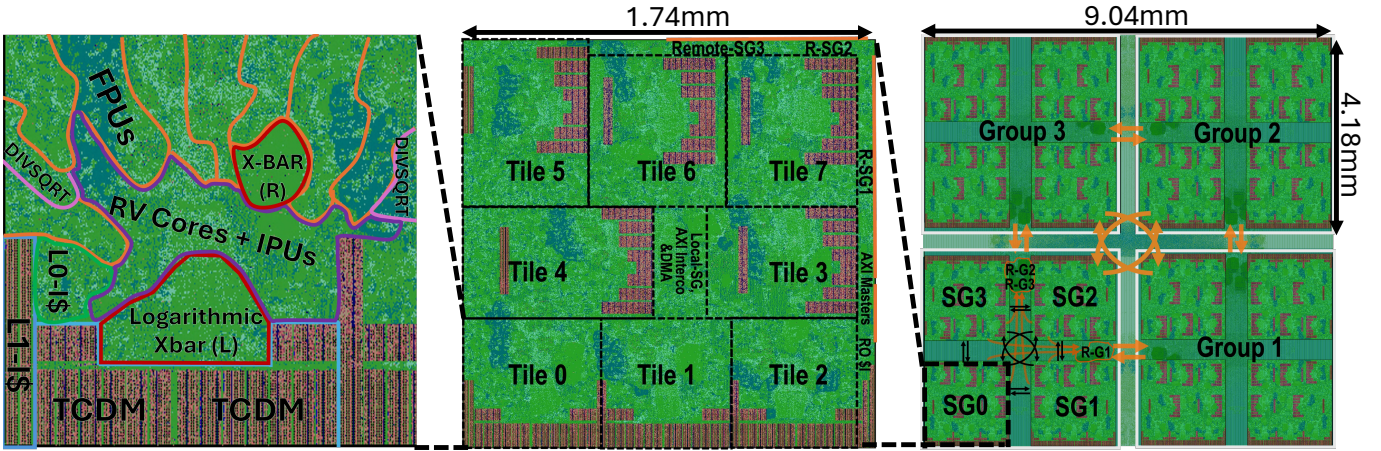


Figure 10. Placed-and-routed layout annotated view of each TeraPool hierarchical instance.

target (TT/0.80 V/25 °C). These findings fully support our insights in Section 3.2 regarding TeraPool’s physically-aware hierarchical interconnect analysis.

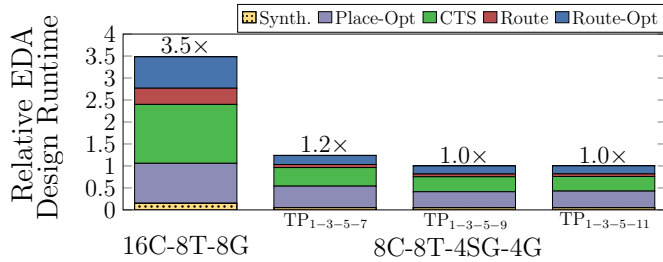


Figure 11. Breakdown of the relative implementation time for TeraPool’s Group in different design configurations.

Fig. 10 shows a snapshot of the physical layout with annotated module placement. The Subgroup is implemented in 3.03 mm<sup>2</sup>, resulting in 0.047 mm<sup>2</sup>/core and a satisfactory 58% area utilization. Each Subgroup comprises 8 Tiles, with the SPM macros of each Tile grouped and placed in a U-shape to enclose the local crossbar, thereby minimizing the overall distance and avoiding excessive macro stacking. The center and edges of the Subgroup are left free to place interconnect cells, and the macros U-shape is rotated on the bottom side to better utilize the design area. The interface ports for remote-Subgroups and remote-Groups are placed on the northeast boundaries. Subgroup and Group blocks are arranged in a point-symmetric grid, with channels in between to PnR the interconnects. To further improve area utilization, we place interface ports behind the Subgroup blocks and shrink the channel width until BEOL resources become limited. At the Cluster top level, 0.68 mm-wide channels are allocated for connecting Groups’ crossbars across the center, and for linking AXI-to-HBM2E channels to boundaries. These routing channels increase the overall area per core to 0.079 mm<sup>2</sup>/core.

### 6.2 Performance and Logic Area

We configure and implement hardware-parameterizable latency for remote Group access with 7-/9-/11-cycle, achieving operating frequencies of 730-/ 850-/910 MHz, respectively (TT/0.80 V/25 °C). These results clearly illustrate the trade-off between latency and operating frequency. When the

configured latency exceeds 11 cycles, the design speed is no longer constrained by the remote Group access path, but by the Snitch core: It starts at a register after the instruction cache, passes through Snitch and a request interconnect, and arrives at the clock gating of an SPM bank.

The Gate Equivalent (GE), defined as the area of a 2-input NAND gate, represents a technology-independent metric for logic area. As shown in Fig. 12, our hierarchical interconnect design accounts for only 8.5% and the HBML occupies a negligible 9.2% of the cluster area. The most significant area component is the SPM banks, followed by the *Snitch* CCs and the instruction cache. The CCs can be further divided into the cores themselves (7.3%), IPU (9.1%), and the highly area-efficient FP-SSs (22%). This breakdown highlights that the majority of the design’s logic area is dedicated to memory and compute resources, with minimal area cost attributed to both PEs-to-L1-memory interconnects and HBML.

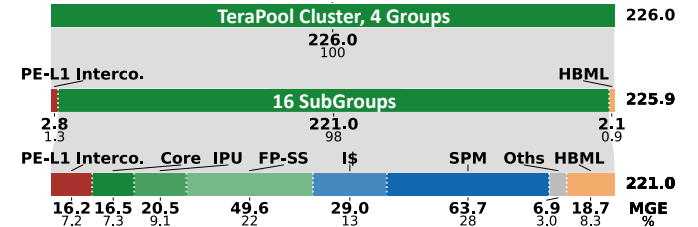


Figure 12. Hierarchical area breakdown with annotations showing the percentage of the immediate parent component.

### 6.3 Energy Analysis

Fig. 13 shows the energy breakdown for instruction execution (pJ/instruction/core) in TeraPool configured with remote Group access latencies of 7-, 9-, and 11 cycles, measured at corresponding operating frequencies of 730-, 850-, and 910 MHz (TT/0.80 V/25 °C). To demonstrate the energy consumption across different memory access distances, we present the energy breakdown for a 32 bit load instruction (*ld*) accessing memory banks within its *local-Tile*, a different *Tile* in the same *SubGroup*, a different *SubGroup* in the same *Group*, and a remote *Group*. With increasing memory access distance, the average energy consumption rises by 10%, 20%, and 58% compared to the *local-Tile*, respectively.

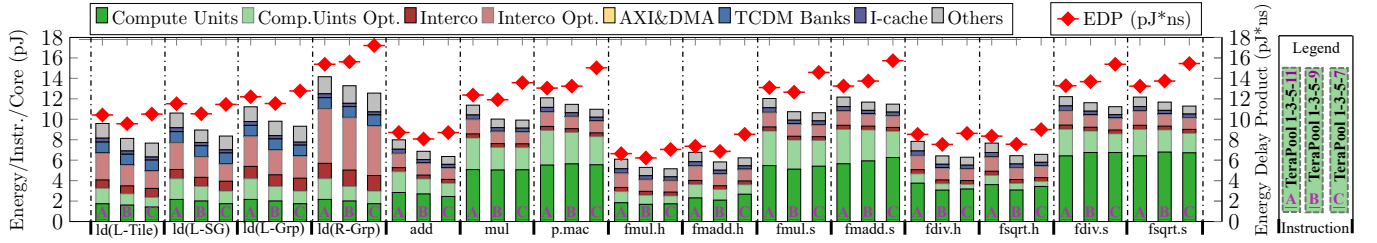


Figure 13. Instruction energy breakdown under typical 0.80 V/25 °C for varying TeraPool configurations (7/9/11 remote Group access latency cycles). Memory access instructions (ld) target local Tile, SubGroup, Group, and remote Group; floating-point instructions presented in single (.s) and half-precision (.h); division/square root energy quantified per DIVSQRT unit.

The interconnect (2.5–6.8 pJ) and L1 SPM banks (1.06 pJ) dominate the energy consumption, contributing up to 51% of the total. For arithmetic instructions, TeraPool consumes 6.4–13.5 pJ for integer operations, 5.2–7.9 pJ for half-precision (16 bit) FP, and 11.3–12.2 pJ for single-precision (32 bit) FP. The computing units (IPU, FP-SS, and DIVSQRT) dominate energy consumption, accounting for an average of 69.9% in integer, 60% in half-precision FP, and 72.3% in single-precision FP computations. When the interconnect crossbars are not accessed, for instance, during the execution of a single-precision FMA (FP Multiply-Add, *fmadd.s*) operation, which consumes 12.19 pJ, only 14.5% of the total power, primarily due to internal cell power from clock propagation and leakage. Thanks to memory clock gating, the SPM banks consume less than 0.1 pJ, achieving a 98% reduction in energy consumption and becoming negligible when not accessed.

The light-colored segments in the plot, adjacent to the *Compute Units* and *Interconnect* segments, represent the energy consumption of optimization cells introduced by physical design to achieve the target frequency. These segments show a slight increase as the frequency rises, driven by the use of low-threshold optimization cells, designed to minimize delay at the expense of higher power consumption, to meet the near-gigahertz operating frequency target. For instance, as the operating frequency increases from 730 MHz to 910 MHz under typical conditions (TT/0.80 V/25 °C), the energy consumption rises by only 1.6 pJ for remote *Group* memory access and 1.4 pJ for single-precision FP multiplication (*fmul*), reflecting an average increase of 16%.

The Energy-Delay Product (EDP) is a key metric that normalizes energy efficiency and delay [29], providing insight into the trade-offs between energy consumption and performance. To identify the optimal energy-performance configuration for TeraPool, we analyze the EDP in pJ × ns for each instruction, highlighted with red markers in Fig. 13. The results clearly show that, for most operations, the TeraPool configuration with a 9-cycle remote *Group* latency operating at 850 MHz achieves the optimal balance between energy efficiency and performance. In summary, TeraPool achieves an energy-efficient design, consuming only 5~15 pJ/operation/core, even for high-complexity 32 bit FP operations, the majority of the energy is spent toward computing components.

## 7 PERFORMANCE ANALYSIS

One advantage of a shared-memory cluster is its programming simplicity compared to managing data transfers across multiple clusters. TeraPool supports a streamlined *fork-join* programming model with C-runtime functions, which

enable efficient transitions between sequential and parallel code sections for Single Program Multiple Data (SPMD) execution [30]. After booting all the PEs execute concurrently the C-binary, the programmer can access PEs' unique ID and statically assign to each core independent tasks in a parallel computation (*fork*). Once PEs complete, they synchronize (*join*) via atomic *fetch&add* to shared memory locations.

To evaluate interconnect performance and overall cluster utilization, the benchmarks cover data-parallel execution with both sequential and non-sequential memory access patterns. For sequential memory access execution, A Times X Plus Y (AXPY) and Dot Product (DOTP) are used as *local-access* kernels, where PEs primarily fetch data from nearby regions of the shared memory with low latency, and inputs are not fetched by more than one core, making them ideal for evaluating the lower-hierarchy interconnect. The General Matrix Multiplications (GEMM) serves as a *global-access* kernel, where data structures are distributed across all shared SPM banks. A tiled implementation is used to fully utilize the register file and maximize computational intensity.

For non-sequential memory accessing, we adopt a radix-4 decimation in frequency Cooley-Turkey Fast Fourier Transform (FFT) to ease the memory accesses in local banks. In the  $k^{th}$  stage of an N-point FFT, each core computes 4 butterflies, taking 4 inputs at a distance of  $N/(4 \times 4k)$ . PEs working on different FFTs are independently synchronized. We also include Sparse Matrix-Matrix Addition (SpMMadd) with CSR format, which performs element-wise addition of two graphs and represents a key *GraphBLAS* operation [31], to evaluate the interconnect under irregular distributed memory accesses.

In Fig. 14 a), we present kernel performance on the most energy-efficient configuration with a 9-cycle remote *Group* latency, operating at 850 MHz (TT/0.80 V/25 °C). We break down the instructions-per-cycle (IPC) and architectural stall fractions as a percentage of total cycles. Since all memory accesses are local, both AXPY and DOTP achieve low AMAT and high IPC values of 0.85 and 0.83, respectively, benefiting from the high bandwidth of the local-*Tile* interconnect. The performance loss is attributed only to the synchronization barrier (wait-for-interrupt (WFI)) at the end of the computation. DOTP incurs more AMAT and synchronization overhead due to the reduction. For GEMM, a global-access-dominated kernel where cores fetch data across the entire cluster, the measured AMAT aligns closely with the random-access analytical model presented in Section 3, validating model accuracy for design guidance. The IPC remains high at 0.7, while a larger fraction of LSU stalls is due to global accesses that require PEs to fetch data from all banks through shared interconnect ports. A

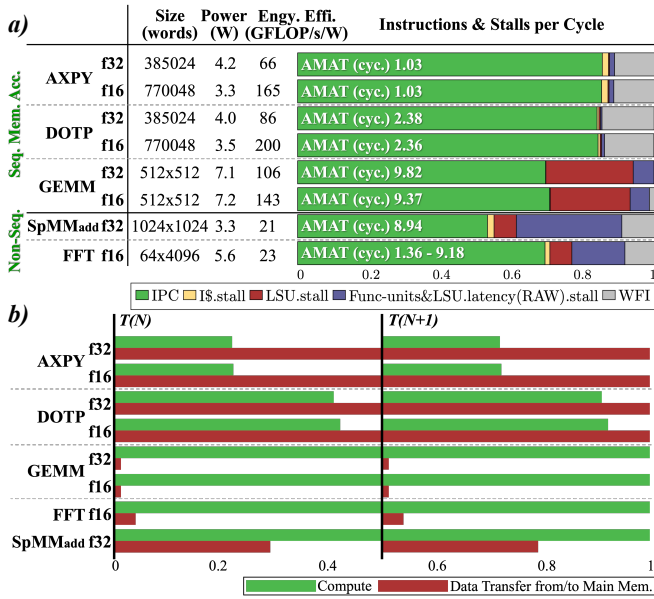


Figure 14. a) Instruction and stall fractions over total cycles for kernel execution in TeraPool; b) Timing breakdown of double-buffered kernels with data transfer to/from HBM2E.

smaller fraction of read-after-write (RAW) stalls arises from increased latency during interconnect conflicts. The negligible synchronization overhead, thanks to our large shared memory, enables the cluster to handle larger problem tiling efficiently.

For non-sequential memory accessing, we run 64 independent 4096-point FFTs in parallel, computing each stage between barriers to minimize overhead. It achieves 0.7 IPC, performing at 23 GFLOP/s/W due to the required data-control instructions such as packaging and shuffling alongside computation. The AMAT ranges from 1.36 to 9.18 cycles across different stages. Data access through interconnects within and between *SubGroups* incurs only 6.15% LSU stalls. Although PEs are not optimized with dedicated extensions for sparse workloads, SpMMadd still achieves a high IPC of 0.53. Frequent conditional branches stress the non-specialized PEs, where the limited number of ISA-defined registers hinders loop unrolling and leads to RAW stalls. However, when analyzing memory accesses, we note that non-sequential narrow accesses incur only 6% interconnect contention, demonstrating our interconnect supports multiple irregular parallel accesses in a non-blocking fashion.

To assess the high bandwidth of TeraPool’s HBML, we benchmark kernels accessing data through industry-standard HBM2E, employing double-buffering to hide transfer latency. We use two L1 buffer spaces: one for executing the current kernel ( $T(N)$ ) and another for transferring data for the next round ( $T(N+1)$ ). As shown in Fig. 14 b), even for heavily memory-bound kernels, DOTP achieves a compute phase of 82%, while AXPY achieves 44%, as fast computation fails to hide the latency of result transfers and new data loads. For compute-bound kernels, TeraPool achieves high performance: its large shared-L1 completely hides the HBM2E latency.

These analyses highlight the capability of our PE-to-L1 interconnect and HBML in delivering a significant fraction of the peak workload, even for kernels with highly global PE-to-L1 traffic patterns, non-negligible contention, and

long-latency data transfers with HBM2E main memory.

## 8 RELATED WORK

In this section, we compare our work with cluster-based, programmable, multi-core and many-core architectures that employ various scaling-up/-out topologies to achieve high core-counts. We privilege algorithmic flexibility, and focus on clusters of general-purpose PEs, in contrast to dense arrays of hyper-specialized, single-domain PEs (e.g., Neural Processing Units (NPU)). Table 5 provides an overview of these architectures. We can divide the state-of-the-art into two main categories: multi-core designs with a cluster’s core count < 100 and many-core designs with > 100.

In the multi-core designs category, we find both scaled-up/-out topologies: (i.) crossbar-based clusters scaling-out via a 2-D mesh NoC with router links such as *Kalray MPPA3-80* [32], and (ii.) scaled-up clusters with crossbar-based interconnects, such as *Ramon RC64* [10], [33]. In the latter, all cores connect to a shared 4 MB SPM employing multistage logarithmic crossbars. The core count is limited to reduce routing complexity. Our work clearly outperforms these designs by virtue of a much larger core count, achieving 32-128 $\times$  performance.

In the many-core design category, among the scaled-out architectures, *TensTorrent’s Wormhole* [34] integrates 400 PEs in a  $10 \times 8$  *Tensix Matrix* interconnected via a 2-D mesh NoC. In each *Tensix* only 5 PEs share 1.5 MB L1 cache through a crossbar with 4 pipeline stages. With the same round-trip pipeline, TeraPool’s *Group* features 256 PEs interconnected to the *Group*-local portion of a 1 MiB shared-memory, achieving a 76.8 $\times$  PEs-to-local-shared-memory ratio, thanks to our single-stage PE design with a fully combinational crossbar, incorporating only spill registers at hierarchical boundaries to break long remote access paths. In *Esperanto ET-SoC-1* [9], a crossbar connects 32 *Minion* cores to a 4 MB L1 cache, scaling out to 1088 cores through a 2-D mesh NoC while utilizes RISC-V Vector (RVV) PEs with a large vector register file to hide transaction latency. TeraPool achieves a similar core count by only scaling up, with latency hidden by a negligible-sized transaction table instead of relying on a power-costly large register file in our lightweight scalar core design. Our design achieves 16 $\times$  higher L1 bandwidth and 32 $\times$  higher L2 bandwidth. *HammerBlade* [35] scales out from a single-core *Tile* with 4 kB SPM, using a mixed 2D-mesh topology: *Tiles* are connected via Half-Ruche channels horizontally, direct mesh links vertically, and wormhole-skipped links between *Cache Tiles* and HBM2 for cache refilling. The shared SPM region (*Tile Group*) is defined at design time within a 128-core *Cell* (up to 0.5 MiB), which is 8 $\times$  smaller than our shared-memory scale. Despite this sophisticated topology, accessing the shared memory can take up to 52 cycles and requires each *Tile* to support up to 63 outstanding requests. In contrast, TeraPool achieves a 46 $\times$  advantage in the ratio of shared-memory size to maximum access latency. As a result, *HammerBlade* demands data-placement-aware programming to mitigate latency penalties, increasing programming complexity.

The *Occamy* [23] scales out from a cluster where 8 RISC-V PEs share a low-latency (1 cycle) 128 KiB L1 memory through a crossbar-based interconnect. To enable parallel processing on large datasets, 24 scaled-out clusters are interconnected, with data managed by DMAs within each cluster and inter-cluster

interconnects occupying 14.8% of the die area. In contrast, TeraPool eliminates inter-cluster interconnects, featuring a  $32\times$  larger L1 size managed by a single DMA, further simplifying programming. Finally, in modern GPUs' SMs, PEs share memory through a crossbar-based interconnect. For instance, NVIDIA's H100 [14], [36] is organized into SMs with 128 FP32 units sharing 256 kB memory, and scales-out via a data-driven NoC mesh to a total of 18 432 PEs. In TeraPool, the shared memory is  $16\times$  larger, with  $4\times$  L1 bandwidth per PE, while remaining physically feasible. Moreover, to support Single Instruction Multiple Threads (SIMT) execution, each SM incorporates multiple schedulers, dispatch units, and large register files, significantly increasing hardware complexity. In contrast, TeraPool's low-latency shared memory with outstanding transaction support avoids reliance on thread switching to hide latency, reducing hardware costs. Additionally, its SPMD execution employs a unified multi-megabyte L1 address space, eliminating the need for shared data replication across separate memory regions.

To our knowledge, the largest scaled-up shared-memory cluster in the literature is MemPool [16]. It follows a design philosophy similar to our work, featuring 256 cores sharing a 1 MiB SPM. With our proposed hierarchical interconnect and physical-design-aware methodology, we scale up the cluster by  $4\times$ , incorporating more powerful PEs with multi-precision FP support. Physical feasibility is maintained, enabling all PEs to access any of the 4096 shared memory banks with only a 2–6 (depending on target frequency) cycle latency increase at most, which is effectively hidden by the PE's non-blocking load/store unit and proper instruction scheduling.

It is possible to quantitatively and fairly compare TeraPool with Occamy and MemPool since they are all open-source architectures, representative of small (tens of PEs), large (hundreds of PEs), ultra-large (thousand PEs) clusters. Table 6 compares the main memory accesses required to sustain the workload per unit computation (Byte/FLOP) and utilization (IPC) for two key kernels, namely AXPY and GEMM. Clearly, we want to minimize the former and maximize the latter. For a kernel with low data reuse like AXPY, the Byte/FLOP remains unchanged across designs. TeraPool, the largest cluster design, achieves the same high utilization (0.85 IPC), as data can be stored close to PEs, to leverage the high-bandwidth of low-latency local interconnects. For GEMM, we see a more complex trade-off: IPC decreases for TeraPool, due to increased latency in the remote *Group* interconnects, and the conflicts at the hierarchy boundaries when cores within the same *Tile* concurrently access the same *Group*. Nevertheless, the IPC remains high at 0.7. On the other hand, the large capacity of TeraPool's memory enables large-scale tiling and more data reuse. The 19% drop in IPC is more than compensated by the 44% and 85% reduction of system-level bandwidth-per-core required to sustain the workload, especially in view of the well-known "Memory Wall" problem.

## 9 CLUSTER SCALE-UP TRADE-OFFS AND FUTURE WORK

While we demonstrate the hardware and software benefits of larger clusters, scaling up introduces two main trade-offs in PE-to-L1-memory interconnects. The first is the floorplan area. Although our interconnect ensures physical

feasibility, it requires routing channels (40% die area) between implementation blocks for crossbar placement and wiring. In contrast, smaller clusters that follow the same design principle, such as MemPool [16], incur lower area overhead due to fewer hierarchical levels. The second trade-off concerns inter-hierarchy bisection bandwidth scaling. A higher peak-to-bisection bandwidth ratio ( $peakBW/bisecBW$ ) indicates more contention when memory accesses are not localized. Compared to MemPool (1 KiB/cycle peak, 0.75 KiB/cycle bisection), TeraPool scales by  $4\times$  with a linearly increased peak bandwidth of 4 KiB/cycle. However, the bisection bandwidth reaches only 1.875 KiB/cycle, constrained by wiring resources, increasing the peak-to-bisection ratio by 60%.

To address these trade-offs, future work will focus on exploring more area-efficient interconnect designs. A promising direction is using 2D-mesh NoCs with over-macro routing [16] for PE-to-L1-memory communication. The mesh regular wiring topology allows exploiting controlled routing on higher metal layers and reduces channel overhead, and the configurable router count allows fully utilizing wiring resources to improve bisection bandwidth. However, as the end-to-end latency increases with hop count, NoCs are less suitable for latency-sensitive core-to-L1-memory access. Combining 2D-mesh networks with crossbars may provide a balanced solution that supports scalability and low latency.

Another direction of evolution is application-oriented architectural customization. While this work presents TeraPool with general-purpose PEs, future deployments may benefit from dedicated ISA extensions or co-processors tailored to specialized workloads and data formats (e.g., sparsity and quantized data formats). Moreover, the local-Tile folded sequential SPM address regions are well-suited for integrating specialized engines, such as tensor arrays or NPUs, to accelerate AI-centric computation.

## 10 CONCLUSION

TeraPool is a physically feasible many-core cluster design featuring 1024 individually programmable, floating-point-capable RISC-V cores sharing 4 MiB of L1 SPM through NUMA hierarchical crossbar interconnects delivering up to 4096 B/cycle bandwidth. The 932 GB/s High-Bandwidth Memory Link is designed to efficiently manage data transfers in/out of the large shared L1. It improves by  $\times 4$  the PE count with respect to the largest state-of-the-art cluster.

Through a comprehensive analysis of the core-L1 interconnect, we successfully placed and routed the cluster using GlobalFoundries' 12LPPLUS FinFET technology. TeraPool delivers 0.27-0.74 TFLOP/s single-precision, and up to 1 TFLOP/s half-precision performance, achieving 23 GFLOP/s/W to 200 GFLOP/s/W energy efficiency on real-world kernels. This work demonstrates that the shared-L1 memory paradigm can scale to a thousand cores while maintaining physical feasibility, providing substantial parallel computing power. The unified-address shared-L1 memory accommodates multi-megabyte data chunks while eliminating the cost of inter-cluster global interconnects, minimizing data transfer, splitting-merging, and synchronization overhead.

Table 5  
Comparison of State-of-the-Art (SoA) Cluster-based Many-core Designs

	Processing Element (PE)	Data Types	Execution Model	No.PEs /Cluster	Total PEs	Shared-L1 (MiB)	L1/L2 Interco. Bandwidth (Byte/Cycle)	L1 Latency (cycles)	Peak (FL)OP /cyc./Cluster <sup>a</sup>	Scaling Topology	Open Source	
<b>Multi-core</b> (No.PEs < 100)	<b>This work</b>	32bit RISC-V	Int32/16-SIMD; FP32/16-SIMD; Complex32 (16b Real&Imag)	<b>SPMD</b>	<b>1024</b>	1024	<b>4</b>	<b>4096/1024</b>	<b>1-11 (NUMA)</b>	<b>2048</b>	<b>Scaling-up Crossbar</b>	<b>Yes</b>
	<b>Kalray MPPA3-80 [32]</b>	64bit VLIW	Int16/8; FP64/32/16	SPMD; LWI	16	80	3.8	64/1024	23	32	Scaling-out 2D-mesh NoC	No
<b>Many-core</b> (No.PEs > 100)	<b>Ramon RC64 [10], [33]</b>	32bit VLIW	Int32/16/8	MIMD	64	64	3.8	1024/N.A.	N.A.	128	Scaling-up Crossbar	No
	<b>TensTorrent [34]</b>	32bit RISC-V	FP32/16/8	SIMD	5	400	1.43	20/N.A.	> 4 <sup>b</sup>	10	Scaling-out 2D-mesh NoC	No
	<b>Wormhole Esperanto ET-SoC-1 [9]</b>	64bit RVV	Int8/N.A.; FP32/16	SIMD	32	1088	3.8	256/32	N.A.	64	Scaling-out 2D-mesh NoC	No
	<b>Nvidia H100 [14]</b>	64/32bit PTX	Int8; FP64/16/8; BF16;TF32	SIMT	128 (SM)	18432	0.244 (SM)	128/N.A.	16.57 <sup>c</sup> (Average)	1736	Scaling-out Data-Driven	No
	<b>Hammer<sup>d</sup> Blade [35]</b>	32bit RISC-V	Int32/-; FP32/-	SPMD	128 (Cell)	2048	0.5 (Cell)	512/N.A.	4+ 2 x hops	256	Scaling-out 2D-ruche NoC	<b>Yes</b>
	<b>Occamy [23]</b>	64bit RISC-V	Int64/32/16-SIMD; FP64/32/16/8-SIMD	SPMD	8	432	0.125	32/256	1	32	Scaling-out Crossbar	<b>Yes</b>
<b>MemPool [16]</b>	32bit RISC-V	Int32/16-SIMD	SPMD	256	256	1	1024/256	1-5 (NUMA)	512	Scaling-up Crossbar	<b>Yes</b>	

<sup>a</sup> In 32-bit operations, one MAC is counted as two operations. <sup>b</sup> A 4-cycle interconnect pipeline with unknown core latency. <sup>c</sup> Benchmarking referenced from <https://chipsandcheese.com/p/nvidias-h100-funny-l2-and-tons-of-bandwidth>, last accessed on Feb. 28, 2025. <sup>d</sup> We assume one *Tile group* per *HB Cell* as a shared-memory cluster, where the *Group* SPM address space is shared across all *Tiles*.

Table 6  
Data Transfer Cost vs. Compute IPC

	Cluster's Max. Tiling (MiB)	Local Data Distrib. Kernel (XPY f32)		Global Data Distrib.** Kernel (MatMul f32)	
		Main Mem. Transfer Byte/FLOP	Comp. IPC	Main Mem. Transfer Byte/FLOP	Comp. IPC
Scaled-up Ultra-Large Cluster (This work*)	4.00	6.00	0.85	0.009	0.70
Scaled-up Large Cluster (MemPool [16]*)	1.00	6.00	0.85	0.016	0.88
Scaled-out Many Clusters (Occamy [23]*)	0.125	6.00	0.85	0.062	0.89

\* Same configuration of PE, transaction table, and instruction cache.

\*\* 8 MiB problem matrices in main memory; tiling based output matrix.

## ACKNOWLEDGMENTS

This work has received funding from the Swiss State Secretariat for Education, Research, and Innovation (SERI) under the SwissChips initiative.

## REFERENCES

- J. Sevilla, L. Heim, A. Ho, T. Besiroglu, M. Hobbhahn, and P. Villalobos, "Compute Trends Across Three Eras of Machine Learning," in *Int. Jt. Conf. Neural Netw.* Padua, Italy: IEEE, July 2022, pp. 1–8.
- X. Zhu, J. Li, Y. Liu, C. Ma, and W. Wang, "A Survey on Model Compression for Large Language Models," *Trans. Assoc. Comput. Linguist.*, vol. 12, no. 1, pp. 1556–1577, Nov. 2024.
- B. Peccerillo, M. Mannino, A. Mondelli, and S. Bartolini, "A survey on hardware accelerators: Taxonomy, Trends, Challenges, and Perspectives," *J. Syst. Archit.*, vol. 129, pp. 1–51, Aug. 2022, article number 102561.
- K. Rupp, "50 Years of Microprocessor Trend Data," GitHub Repo., 2022, [Online]. Available: <https://github.com/karlrupp/microprocessor-trend-data>.
- G. Singh *et al.*, "Near-memory Computing: Past, Present, and Future," *Microprocess. Microsyst.*, vol. 71, pp. 1–15, Aug. 2019, article number 102868.
- R. Muralidhar, R. Borovica-Gajic, and R. Buyya, "Energy Efficient Computing Systems: Architectures, Abstractions and Modeling to Techniques and Standards," *ACM Comput. Surv.*, vol. 54, no. 11, pp. 1–37, sep 2022.
- M. Horowitz, "Computing's Energy Problem (and What We Can Do About It)," in *IEEE Int. Solid-State Circuits Conf. Dig. Tech. Pap.* San Francisco, CA, USA: IEEE, Feb. 2014, pp. 10–14.
- M. Ishii, J. Detrey, P. Gaudry, A. Inomata, and K. Fujikawa, "Fast Modular Arithmetic on the Kalray MPPA-256 Processor for an Energy-Efficient Implementation of ECM," *IEEE Trans. Comput.*, vol. 66, no. 12, pp. 2019–2030, May 2017.
- D. R. Ditzel *et al.*, "Accelerating ML Recommendation With Over 1,000 RISC-V/Tensor Processors on Esperanto's ET-SoC-1 Chip," *IEEE Micro*, vol. 42, no. 3, pp. 31–38, Jan. 2022.
- R. Ginosar *et al.*, "Ramon Space RC64-based AI/ML Inference Engine," in *Eur. Workshop On-Board Data Process.* Online Event: ESA-ESTEC, Jun 2021, pp. 1–33.
- S. Lie, "Multi-Million Core, Multi-Wafer AI Cluster," in *IEEE Hot Chips Symp.* Palo Alto, CA, USA: IEEE, Aug. 2021, pp. 1–41.
- W. Lang, S. Harizopoulos, J. M. Patel, M. A. Shah, and D. Tsirogiannis, "Towards energy-efficient database cluster design," *ACM Proceedings of the VLDB Endow.*, vol. 5, no. 11, p. 1684–1695, July 2012.
- NVIDIA Corp., "NVIDIA A100 Tensor Core GPU Architecture," NVIDIA Corp., Tech. Rep., 2020, [Online]. Available: <https://images.nvidia.com/aem-dam/en-zz/Solutions/data-center/nvidia-ampere-architecture-whitepaper.pdf>.
- , "NVIDIA H100 Tensor Core GPU Architecture," NVIDIA Corp., Tech. Rep., 2023, [Online]. Available: <https://resources.nvidia.com/en-us-tensor-core>.
- H. Luan and A. Gatherer, "Combinatorics and Geometry for the Many-ported, Distributed and Shared Memory Architecture," in *IEEE/ACM Int. Symp. Netw.-on-Chip.* Hamburg, Germany: IEEE, Nov. 2020, pp. 1–6.
- S. Riedel, M. Cavalcante, R. Andri, and L. Benini, "MemPool: A Scalable Manycore Architecture with a Low-Latency Shared L1 Memory," *IEEE Trans. Comput.*, vol. 72, no. 12, pp. 3561–3575, Aug. 2023.
- Y. Zhang, S. Riedel, M. Bertuletti, A. Vanelli-Coralli, and L. Benini, "TeraPool-SDR: An 1.89TOPS 1024 RV-Cores 4MiB Shared-L1 Cluster for Next-Generation Open-Source Software-Defined Radios," in *Great Lakes Symp. VLSI.* Clearwater FL USA: ACM, June 2024, pp. 86–91.
- L. Steiner, M. Jung, F. S. Prado, K. Bykov, and N. Wehn, "DRAMSys4.0: An Open-Source Simulation Framework for In-depth DRAM Analyses," *Int. J. Parallel Program.*, vol. 50, no. 2, pp. 217–242, April 2022.
- H. T. Kung, "Memory Requirements for Balanced Computer Architectures," *SIGARCH Comput. Archit. News*, vol. 14, no. 2, pp. 49–54, May 1986.
- J. Ma, G. Yan, Y. Han, and X. Li, "An Analytical Framework for Estimating Scale-Out and Scale-Up Power Efficiency of Heterogeneous Manycores," *IEEE Trans. Comput.*, vol. 65, no. 2, pp. 367–381, April 2016.
- J. Dean and L. A. Barroso, "The Tail at Scale," *Commun. ACM*, vol. 56, no. 2, pp. 74–80, Feb. 2013.

- [22] R. M. Radway, A. Bartolo, P. C. Jolly *et al.*, "Illusion of Large On-Chip Memory by Networked Computing Chips for Neural Network Inference," *Nat. Electron.*, vol. 4, no. 1, pp. 71–80, Jan. 2021.
- [23] P. Scheffler *et al.*, "Occamy: A 432-Core Dual-Chiplet Dual-HBM2E 768-DP-GFLOP/s RISC-V System for 8-to-64-bit Dense and Sparse Computing in 12-nm FinFET," *IEEE J. Solid-State Circuits*, pp. 1–15, Jan. 2025, early access.
- [24] X. Li, Z. Li, Y. Ju, X. Zhang, R. Wang, and W. Zhou, "COP: A Combinational Optimization Power Budgeting Method for Manycore Systems in Dark Silicon," *IEEE Trans. Comput.*, vol. 72, no. 5, pp. 1356–1370, Oct. 2023.
- [25] X. Zhao, S. Ma, Z. Wang, N. E. Jerger, and L. Eeckhout, "CD-Xbar: A Converge-Diverge Crossbar Network for High-Performance GPUs," *IEEE Trans. Comput.*, vol. 68, no. 9, pp. 1283–1296, March 2019.
- [26] L. Bertaccini, G. Paulin, M. Cavalcante, T. Fischer, S. Mach, and L. Benini, "MiniFloats on RISC-V Cores: ISA Extensions with Mixed-Precision Short Dot Products," *IEEE Trans. Emerg. Top. Comput.*, vol. 12, no. 4, pp. 1040–1055, Feb. 2024.
- [27] S. Ristov, M. Gusev, and G. Velkoski, "Optimal Block Size for Matrix Multiplication Using Blocking," in *Int. Conv. Inf. Commun. Technol. Electron. Microelectron.* Opatija, Croatia: IEEE, July 2014, pp. 295–300.
- [28] T. Benz *et al.*, "A High-Performance, Energy-Efficient Modular DMA Engine Architecture," *IEEE Trans. Comput.*, vol. 73, no. 1, pp. 263–277, Jan. 2024.
- [29] W. Choi *et al.*, "On-Chip Communication Network for Efficient Training of Deep Convolutional Networks on Heterogeneous Manycore Systems," *IEEE Trans. Comput.*, vol. 67, no. 5, pp. 672–686, Nov. 2018.
- [30] J. Diaz, C. Muñoz-Caro, and A. Niño, "A Survey of Parallel Programming Models and Tools in the Multi and Many-Core Era," *IEEE Trans. Parallel Distrib. Syst.*, vol. 23, no. 8, pp. 1369–1386, Jan. 2012.
- [31] J. Kepner *et al.*, "Mathematical foundations of the GraphBLAS," in *HPEC*. Waltham, MA, USA: IEEE, Dec. 2016, pp. 1–9.
- [32] B. D. de Dinechin, *A Qualitative Approach to Many-Core Architecture*. Hoboken, New Jersey, USA: Wiley, April 2021, ch. 2, pp. 27–51.
- [33] R. Ginosar, P. Aviely, T. Israeli, and H. Meirov, "RC64: High Performance Rad-Hard Manycore," in *IEEE Aerosp. Conf.* Big Sky, MT, USA: IEEE, March 2016, pp. 1–9.
- [34] J. Vasiljevic, L. Bajic, D. Capalija, S. Sokorac, D. Ignjatovic, and D. et al., Thompson, "Compute Substrate for Software 2.0," *IEEE Micro*, vol. 41, no. 2, pp. 50–55, March 2021.
- [35] D. C. Jung, M. Rutenberg, P. Gao, S. Davidson, D. Petrisko, and M. B. et al., Taylor, "Scalable, Programmable and Dense: The HammerBlade Open-Source RISC-V Manycore," in *ISCA*. Buenos Aires, Argentina: ACM/IEEE, Aug. 2024, pp. 770–784.
- [36] Z. Jin *et al.*, "Uncovering Real GPU NoC Characteristics: Implications on Interconnect Architecture," in *IEEE/ACM Int. Symp. Microarchitect.* Austin, TX, USA: IEEE, Nov. 2024, pp. 885–898.



**Chi Zhang** received his B.Sc. degree from Huazhong University of Science and Technology China in 2019 and his M.Sc. degree from KTH Royal Institute of Technology Sweden in 2022. He is currently pursuing a Ph.D. degree in the Digital Circuits and Systems group of Prof. Benini. His research interests include high-performance computing, memory systems, and near-memory computing.



**Samuel Riedel** received his B.Sc. and M.Sc. degrees in Electrical Engineering and Information Technology at ETH Zurich in 2017 and 2019, respectively. He is currently pursuing a Ph.D. degree in the Digital Circuits and Systems group of Prof. Benini. His research interests include computer architecture, focusing on manycore systems and their programming model.



**Diyou Shen** received his B.Sc. degree from University of Colorado Boulder in 2021 and his M.Sc. degree in Electrical Engineering and Information Technology from ETH Zurich in 2024. He is currently pursuing a Ph.D. degree in the Digital Circuits and Systems group of Prof. Benini. His research interests include high-performance computing and fault-tolerance interconnection.



**Bowen Wang** received his B.Sc. degree from Harbin Institute of Technology in 2021 and M.Sc. degrees in Electrical Engineering and Information Technology at ETH Zurich in 2024. He is currently pursuing a Ph.D. degree in the Digital Circuits and Systems group of Prof. Benini. His research interests include computer architecture, flexible manycore systems and neural network deployment.



**Yichao Zhang** received his B.Eng. degree from Heilongjiang University China in 2015 and his M.Sc. degree from Nanyang Technological University Singapore in 2017. He served in the physical VLSI design at Cadence Design Systems and MediaTek Singapore until 2021. He is currently pursuing a Ph.D. degree in the Digital Circuits and Systems group of Prof. Benini. His research interests include physically feasible, many-core parallel computing architectures, and SIMD processing.



**Alessandro Vanelli-Coralli** is Full Professor at the Università di Bologna and is a Senior Scientist at ETH Zürich. His research activity focuses on Wireless Communication with specific emphasis on Satellite Communications. He participates in national and international research projects on satellite mobile communication systems and Prime Contractor for several European Space Agency and European Commission funded projects. Dr. Vanelli-Coralli has been the general co-chairman of the IEEE ASMS Conference since 2010.



**Marco Bertuletti** received his B.Sc. and M.Sc. degrees in Electrical Engineering at Politecnico di Milano, Milano, Italy. He is currently pursuing a Ph.D. degree in the Digital Circuits and Systems group of Prof. Benini. His research interests include the design of multi and Many-Core clusters of RISC-V processors for next-generation telecommunications.



**Luca Benini** holds the chair of digital Circuits and systems at ETHZ and is Full Professor at the Università di Bologna. He received a PhD from Stanford University. His research interests are in energy-efficient parallel computing systems, smart sensing micro-systems and machine learning hardware. He is a fellow of the ACM, a member of the Academia Europaea and of the Italian Academy of Engineering and Technology.